On diversity reception of narrow-band 16 star-QAM in fast Rician fading

doi: 10.1109/25.653066

On Diversity Reception of Narrowband 16 STAR-QAM in Fast Rician Fading

Tjeng Thiang Tjhung, *Senior Member, IEEE,* Xiaodai Dong, Fumiyuki Adachi, *Senior Member, IEEE,* and Kang Hai Tan

***Abstract*— An expression for the bit-error rate (BER) of 16 STAR-quadrature amplitude modulation (QAM) with differential encoding and detection in a Rician fading channel with diversity reception is obtained. Two types of intermediate frequency (IF) filters are considered in the analysis: the intersymbol interference (ISI)-free matched and nonISI-free Gaussian filters. BER curves for various ratios of the line-of-sight (LOS) power to the multipath power, Doppler spread frequencies, and orders of diversity are presented. It is shown that 16 STAR-QAM outperforms 16 DPSK under the same power-limited condition. For the Gaussian receive filter, a filter bandwidth of about 1.2 times the symbol rate is found to lead to a minimum error probability prior to the appearance of error-rate floors.**

***Index Terms*— Bit-error rate, diversity reception, quadrature amplitude modulation, Rician fading.**

I. Introduction

A QUADRATURE amplitude modulation (QAM) scheme called the 16 STAR-QAM with differential encoding and detection has been considered recently to increase bandwidth efficiency in mobile radio. This modulation scheme makes use of eight evenly spaced phases and two amplitudes producing 16 phase-amplitude transitions. In comparison, 16 SQUARE-QAM requires coherent detection, which is difficult to achieve because of fast variations in the received faded signal. Recent advances in amplifier linearization [7] have also made QAM signal formats, with varying signal envelope, a more viable proposition. This is in contrast to the usual preference of using continuous-phase modulation (CPM) schemes, which have constant envelope when faced with the need of class-C power amplification.

A typical fading model in land mobile radio is Rayleigh fading. This model is suitable for urban areas, which are characterized by many obstacles such as buildings surrounding the mobile station; a line-of-sight (LOS) path seldom exists. However, in suburban areas, often a LOS path is produced, which results in a Rician fading channel. This may also be true for microcellular systems with cells of less than several hundred meters in radius and for satellite mobile channels. Rician fading is characterized by the K factor, which is the power ratio of the specular and the diffused components. It represents Rayleigh fading when $K = 0$ and no fading when $K \to \infty$. Rician fading, thus, can be considered a general fading model for both land and satellite mobile channels.

The bit-error rate (BER) performance of 16 STAR-QAM in *Rayleigh* fading has been analyzed by Adachi *et al.* [3] and Chow *et al.* [4]. In [3], a comparison is made between 16 STAR-QAM and 16 SQUARE-QAM, while in [4] an optimum ratio of the two amplitude values is obtained. Recently, Chow *et al.* [5] presented the BER for 16 STAR-QAM in Rayleigh fading, with postdetection combining. In this paper, we present a derivation and computation of the BER performance of 16 STAR-QAM in "LOS plus Rayleigh" or *Rician* fading channel with diversity reception. Performance analysis of Rayleigh fading is therefore just a special case of the formulas derived with $K = 0$. The effect of intermediate frequency (IF) bandlimitation on the error performance of 16 STAR-QAM has not been considered in [3]–[5]. This issue will be investigated in our work.

II. Signal and System Model

16 STAR-QAM is a combination of an independent set of an 8DPSK and a binary differential AM. The transmitted carrier signal with unity power can be expressed in the low-pass equivalent complex form as

$$s(t) = \sum_n A_n \exp(j\theta_n) \cdot p(t - nT). \tag{1}$$

The pulse $p(t)$ has a unit value between interval $[0, T]$ and zero elsewhere. For the nth signaling interval $(n-1)T < t < nT$, $s_n = A_n \exp j\theta_n$, where

$$A_n = \{r_L, r_H\}, \theta_n = \{\theta_0 + m\pi/4, m = 0 - 7\}$$

and θ_0 is the initial phase of the carrier. Assuming equiprobable transmission of amplitude bits, $r_L = \sqrt{2/(1+\beta^2)}$ and $r_H = \beta r_L$ so that $(r_L^2 + r_H^2)/2 = 1$. $\beta = r_H/r_L > 1$ is the amplitude ratio. The set of four binary message bits $\{a_n, b_n, c_n, d_n\}$ is encoded into the nth symbol according to $\Delta r_n \exp(j\Delta\theta_n)$, where $\Delta\theta_n = \theta_n - \theta_{n-1}$ and $\Delta r_n = A_n/A_{n-1}$. Gray encoding of $\{a_n, b_n, c_n\}$ to $\Delta\theta_n$ is assumed for the 8DPSK. For the amplitude modulation, if $d_n = 1, \to \Delta r_n = \beta$ or β^{-1}, depending on the previous amplitude. If $d_n = 0, \to \Delta r_n = 1$.

The transmitted signal is received via a Rician fading channel by an uncorrelated L-branch diversity receiver. The received signal $z(t)$ is the sum of a LOS or specular and

Manuscript received January 27, 1995; revised October 15, 1996.

T. T. Tjhung, X. Dong, and K. H. Tan are with the Department of Electrical Engineering, National University of Singapore, 0511 Singapore.

F. Adachi is with NTT Mobile Communications Network, Inc., Yokosuka-shi, Kanagawa-ken 238-03, Japan.

Publisher Item Identifier S 0018-9545(97)05121-9.

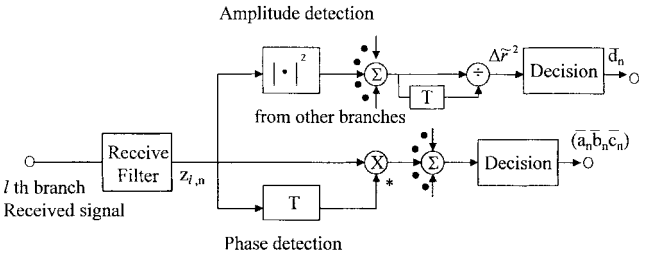

Fig. 1. L-branch diversity receiver.

Rayleigh-faded, multipath, or diffused components

$$z(t) = \sqrt{2P_s}s(t)\exp(-j2\pi f_d t) + \sqrt{P_d}\cdot\mu_s(t) \cdot s(t) + w(t) \quad (2)$$

where P_s and P_d are, respectively, the power of the LOS and multipath components. We assume that the fading rate is much slower than the symbol rate $1/T$ and that there is no time delay between the LOS and the multipath components. The parameter f_d is the Doppler shift of the LOS component. The function $\mu_s(t)$ is a zero-mean complex Gaussian random process describing the fading phenomenon. Considering the arrival of many multipath waves having identical amplitudes and from all directions with equal probability, the power spectrum of $\mu_s(t)$ is given by [12]

$$S(f) = \frac{P_d/\pi}{\sqrt{f_D^2 - f^2}}$$

where f_D is the maximum Doppler frequency given by the mobile moving speed divided by the carrier wavelength. This maximum Doppler frequency f_D, with a subscript of capital case D, is to be distinguished from the Doppler frequency of the LOS component f_d with a subscript of lowercase d.

We assume that the receiver contains an automatic frequency control unit that compensates the Doppler shift, which is equivalent to multiplying all terms in (2) with $\exp(j2\pi f_d t)$. The noise $w(t)$ being white is not affected by a frequency shift, therefore, we shall leave $w(t)$ unchanged. We shall analyze two types of an IF receive filter, as shown in Fig. 1: 1) an ideal matched filter and 2) a Gaussian filter.

III. Case A: Ideal Matched Filter

We consider here a matched filter with a square-pulse response

$$p'(t) = \begin{cases} 1/T, & 0 \le t \le T \\ 0, & \text{elsewhere.} \end{cases}$$

This response is realized by a one-symbol integrate-sample-and-dump (I&D) filter. Assuming that signal symbol timing is ideally locked to the received specular component, the received signal sampled at $t = nT$ can be expressed as

$$z_{l,n} = (\sqrt{2P_s} + \sqrt{P_d}\mu_{s,n}e^{j2\pi f_d(nT)})s_n + w_{l,n} \quad (3)$$

for the lth branch $(l = 1, 2, \cdots, L)$, where $\mu_{s,n}$ is a zero-mean complex Gaussian random variable with $\frac{1}{2}\langle|\mu_{s,n}|^2\rangle = 1$, which accounts for the fading phenomenon $\mu_s(t)$. In (3), the inclusion of the factor $\exp[j2\pi f_d(nT)]$ with the multipath component is a result of: 1) the multiplication of $\exp(j2\pi f_d t)$ to (2) by the receiver Doppler shift compensation process mentioned earlier and 2) the assumption that the fading process is slow compared to the symbol rate so that during the matched filter processing of the received signal in the interval between $(n-1)T$ to nT, $\exp(j2\pi f_d t') \cong \exp(j2\pi f_d nT)$. Finally, $w_{l,n}$ is the sample of a filtered additive white Gaussian noise (AWGN) with variance $2P_n$, that is, $\frac{1}{2}\langle|w_{l,n}|^2\rangle = P_n$ power of the filtered AWGN.

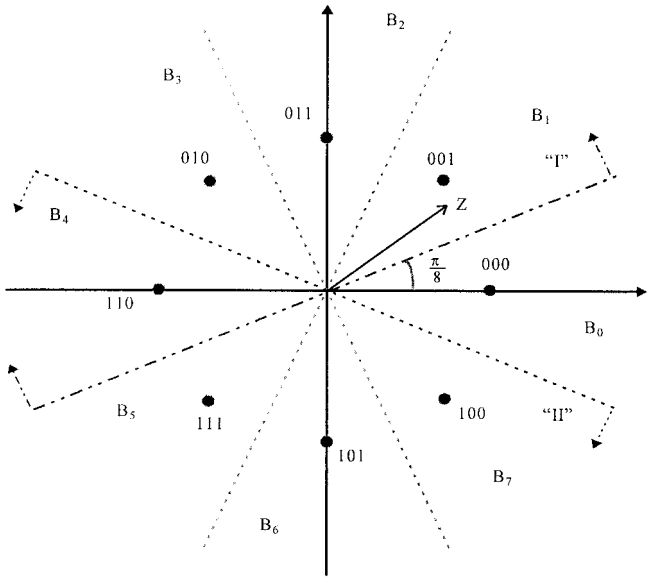

Fig. 2. 8DPSK signal space with optimum decision regions.

The receiver for the differential detection of a 16 STAR-QAM signal can be splitted into two stages: phase detection and amplitude detection. The receiver diagram is shown in Fig. 1.

A. Phase-Detection Error Probability

Let

$$\text{SNR} = (P_s + P_d)/P_n, \quad K = P_s/P_d, \quad \text{and}$$
$$\Gamma = P_d/P_n = \text{SNR}/(1+K).$$

Another signal-to-noise ratio (SNR) γ_b is defined as the average bit energy divided by the AWGN one-sided noise spectral density N_0. This γ_b can be written as $\gamma_b = E_b/N_0 = \text{SNR}/4$, which can be deduced from the fact that the matched filter has an equivalent noise bandwidth of $B = 1/T$, the symbol rate. For the diversity reception, as shown in Fig. 1, the decision on the 8DPSK symbol is based on the decision variable

$$Z = \sum_{l=1}^{L} z_{l,n}z_{l,n-1}^* = |Z|\exp(j\Delta\varphi)$$

where L is the diversity order and $\Delta\varphi$ is the detected differential phase of the two adjacent symbols. On the complex Z-plane, eight symmetric decision regions are chosen to decide on the transmitted differential phase $\Delta\theta_n$. Suppose $\Delta\theta_n = 0$ is sent. Then if Z falls in the region B_0 in Fig. 2, which is bounded by $-\pi/8 \le \Delta\varphi \le \pi/8$, a correct

decision is declared. Error regions are $\Sigma_{n=1}^{7} B_n$, which can also be viewed as half-plane "I" ($\Sigma_{n=1}^{4} B_n$) plus half-plane "II" ($\Sigma_{n=4}^{7} B_n$) minus the overlapped area B_4. Following the method described in [1], the upper bound of the phase-detection error probability can be represented as the sum of probabilities for the two half-planes "I" and "II." If half-plane "I" is counterclockwisely rotated with $3\pi/8$ and half-plane "II" clockwisely rotated with $3\pi/8$, it is easily seen that error probability of phase detection is given by

$$P_{e,\text{phase}} \le P\left(\text{Re}\left[\left(\sum_{l=1}^{L} z_{l,n} z_{l,n-1}^{*}\right) e^{-j(3\pi/8)}\right] < 0\right) + P\left(\text{Re}\left[\left(\sum_{l=1}^{L} z_{l,n} z_{l,n-1}^{*}\right) e^{j(3\pi/8)}\right] < 0\right). \tag{4}$$

Now, define phase decision variable

$$D(\chi) = \text{Re}\left[\left(\sum_{l=1}^{L} z_{l,n} z_{l,n-1}^{*}\right) e^{j\chi}\right]. \tag{5}$$

This is a special case of a general quadratic form in complex-valued Gaussian random variables defined in [2, (1)], which is given by

$$D = \sum_{l=1}^{L} [A|X_l|^2 + B|Y_l|^2 + CX_l^* Y_l + C^* X_l Y_l^*] \tag{6}$$

with $A = 0,\ B = 0$, and $C = e^{j\chi}$. The rotation angle χ of the two half planes, when $\Delta\theta_n = 0$, is $3\pi/8$ and $-3\pi/8$, respectively. It is shown in [2] that

$$\begin{aligned} &P(D<0, |A_n, A_{n-1}) \\ &\quad = Q(a,b) - I_0(ab)e^{-(a^2+b^2/2)} + \frac{I_0(ab)e^{-(a^2+b^2/2)}}{(1+\nu_2/\nu_l)^{2L-1}} \\ &\qquad \cdot \sum_{k=0}^{L} \binom{2L-1}{k} \left(\frac{\nu_2}{\nu_1}\right)^k + \frac{e^{-(a^2+b^2/2)}}{(1+\nu_2/\nu_1)^{2L-1}} \\ &\qquad \cdot \sum_{n=1}^{L-1} I_n(ab) \left\{ \sum_{k=0}^{L-1-n} \binom{2L-1}{k} \right. \\ &\qquad \left. \times \left[\left(\frac{b}{a}\right)^n \left(\frac{\nu_2}{\nu_1}\right)^k - \left(\frac{a}{b}\right)^n \left(\frac{\nu_2}{\nu_1}\right)^{2L-1-k} \right] \right\}, \\ &\qquad L > 1 \\ &P(D<0, |A_n, A_{n-1}) \\ &\quad = Q(a,b) - \frac{\frac{\nu_2}{\nu_1}}{1+\frac{\nu_2}{\nu_1}} I_0(ab)e^{-(a^2+b^2/2)}, \qquad L = 1 \end{aligned} \tag{7}$$

where $Q(a,b)$ is the Marcum Q-function and $I_n(x)$ is the nth order modified Bessel function. In (7)

$$\begin{aligned} a &= \left(\frac{2\nu_1^2\nu_2(\alpha_1\nu_2 - \alpha_2)}{(\nu_1+\nu_2)^2}\right)^{1/2} \\ b &= \left(\frac{2\nu_1\nu_2^2(\alpha_1\nu_1 + \alpha_2)}{(\nu_1+\nu_2)^2}\right)^{1/2} \\ \nu_{2,1} &= \sqrt{w^2 + \frac{1}{|e^{j\chi}|^2(m_{xx}m_{yy} - |m_{xy}|^2)}} \pm w \\ w &= \frac{2\,\text{Re}\,(e^{j\chi}m_{xy}^*)}{2|e^{j\chi}|^2(m_{xx}m_{yy} - |m_{xy}|^2)} \\ \alpha_1 &= |e^{j\chi}|^2[|E(z_{l,n-1})|^2 m_{yy} + |E(z_{l,n})|^2 m_{xx} \\ &\quad - 2\,\text{Re}\,(E(z_{l,n-1})E(z_{l,n})^* m_{xy}^*)] \\ \alpha_2 &= 2\,\text{Re}\,(E(z_{l,n-1})^* E(z_{l,n}) e^{j\chi}) \end{aligned} \tag{8}$$

where m_{xx}, m_{yy}, and m_{xy} are the second moments (central) of the complex-valued Gaussian variables $x = z_{l,n-1}$ and $y = z_{l,n}$

$$\begin{aligned} m_{xx} &= A_{n-1}^2\Gamma + 1, \quad m_{yy} = A_n^2\Gamma + 1 \\ m_{xy} &= A_n A_{n-1}\Gamma\xi_s^*(T)e^{-j2\pi f_d T}e^{-j\Delta\theta_n} + \xi_n^*(T) \\ E(z_{l,n}) &= A_n\sqrt{K\Gamma}e^{j\theta_n}, \quad E(z_{l,n-1}) = A_{n-1}\sqrt{K\Gamma}e^{j\theta_{n-1}} \end{aligned} \tag{9}$$

where $\xi_x(T)$ is the autocorrelation of the fading process and $\xi_n(T)$ is the autocorrelation of the AWGN ($\xi_n(T) = 0$ for the matched filter case). For the fading channel model assumed in Section II, we have

$$\xi_s(T) = \tfrac{1}{2}\langle|\mu_{s,n}\mu_{s,n-1}^*|^2\rangle = J_0(2\pi f_D T)$$

where $J_0(\cdot)$ is the zero-order Bessel function of the first kind. In the above expressions, all means are normalized to $\sqrt{2P_n}$ and all second moments are normalized to $2P_n$. From (4), see (10), given at the bottom of the page.

B. Amplitude-Detection Error Probability

The amplitude bit is detected and decoded based on the amplitude ratio

$$\Delta\tilde{r} = \sqrt{\sum_{l=1}^{L}|z_{l,n}|^2 \Big/ \sum_{l=1}^{L}|z_{l,n-1}|^2}. \tag{11}$$

Let the decision threshold be Δr_L and Δr_H, where $\beta^{-1} < \Delta r_L < 1$ and $1 < \Delta r_H < \beta$. In [5], these decision thresholds are assumed to be related according to $\Delta r_L = 1/\Delta r_H$. We also adopt this assumption in our computations. A decoding error is produced when $\Delta\tilde{r}$ falls outside of

$$\begin{aligned} P_{e,\text{phase}} = 0.25 * &\left(\begin{array}{c} P(D\chi)<0, |r_L, r_L) + P(D(\chi)<0, |r_L, r_H) \\ +P(D(\chi)<0, |r_H, r_L) + P(D(\chi)<0, |r_H, r_H) \end{array} \right)\Big|_{\chi=3\pi/8} \\ + 0.25 * &\left(\begin{array}{c} P(D(\chi)<0, |r_L, r_L) + P(D(\chi)<0, |r_L, r_H) \\ +P(D(\chi)<0, |r_H, r_L) + P(D(\chi)<0, |r_H, r_H) \end{array} \right)\Big|_{\chi=-3\pi/8}. \end{aligned} \tag{10}$$

$(\Delta r_L, \Delta r_H)$, if $A_n = A_{n-1}$, that is if the transmitted amplitude ratio $\Delta r_n = 1$. A decoding error is also produced when $\Delta\tilde{r}$ falls inside of $(\Delta r_L, \Delta r_H)$, if $A_n \neq A_{n-1}$, that is if the transmitted amplitude ratio $\Delta r_n = \beta$ or β^{-1}. In this paper, we will adopt this decision rule.

The amplitude detection error probability is now

$$P_{e,\text{amp}} = \tfrac{1}{4}\left(P_e(HH)+P_e(LL)+P_e(HL)+P_e(LH)\right) \quad (12)$$

where $P_e(LH)$ represents the conditional amplitude error probability for an amplitude sequence going from low to high. The four terms in (12) can be written as follows:

$$\begin{aligned} P_e(HL) &= P_e(LH) = P(\Delta\tilde{r} > \Delta r_L) - P(\Delta\tilde{r} > \Delta r_H) \\ P_e(HH) &= P_e(LL) = P(\Delta\tilde{r} > \Delta r_H) + P(\Delta\tilde{r} < \Delta r_L). \end{aligned} \quad (13)$$

The terms $\Delta\tilde{r} > \Delta r$ can be transformed into

$$(\Delta r)^2 \sum_{l=1}^{L} |z_{l,n-1}|^2 - \sum_{l=1}^{L} |z_{l,n}|^2 < 0.$$

Now, define an amplitude decision variable

$$D(\Delta r) = (\Delta r)^2 \sum_{l=1}^{L} |z_{l,n-1}|^2 - \sum_{l=1}^{L} |z_{l,n}|^2. \quad (14)$$

This is also a special case of a general quadratic form in complex-valued Gaussian random variables defined in (6), with $A = (\Delta r)^2$, $B = -1$, and $C = 0$. The probability, $P(D(\Delta r) < 0, |A_n, A_{n-1})$, has the same expression as (7), but some variables in (8) have different definitions as follows:

$$\begin{aligned} \nu_{2,1} &= \sqrt{w^2 + ((\Delta r)^2(m_{xx}m_{yy} - |m_{xy}|^2))^{-1}} \pm w \\ w &= \frac{(\Delta r)^2 m_{xx} - m_{yy}}{2(\Delta r)^2(m_{xx}m_{yy} - |m_{xy}|^2)} \\ \alpha_1 &= (\Delta r)^2(|E(z_{l,n-1})|^2 m_{yy} + |E(z_{l,n})|^2 m_{xx} \\ &\quad - 2\,\text{Re}\,(E(z_{l,n})^* E(z_{l,n-1}) m_{xy}^*)) \\ \alpha_2 &= (\Delta r)^2 |E(z_{l,n-1})|^2 - |E(z_{l,n})|^2 \end{aligned} \quad (15)$$

where m_{xx}, m_{yy}, and m_{xy} are the second moments of the complex-valued Gaussian variables x and y as shown in (9). Thus, from (12)–(14), see (16), given at the bottom of the page.

C. Bit-Error Rate Performance

Because the amplitude and phase-detection processes are independent, we calculate the BER's of amplitude detection and phase detection separately for obtaining the average BER

$$P_b = 1/4 \cdot P_{b,\text{amp}} + 3/4 \cdot P_{b,\text{phase}}$$

where $P_{b,\text{amp}}$ and $P_{b,\text{phase}}$ are the BER's of amplitude and phase bits, respectively. This is a weighted sum of the BER for the amplitude and phase detection. Remembering that the phase modulation is a Gray-coded eight-level modulation, while the amplitude modulation is a binary modulation

$$P_{b,\text{amp}} = P_{e,\text{amp}} \quad \text{and} \quad P_{b,\text{phase}} = (P_{e,\text{phase}})/3.$$

Consequently

$$P_b = \tfrac{1}{4}\left(P_{e,\text{amp}} + P_{e,\text{phase}}\right). \quad (17)$$

IV. Case B: NonISI-Free Gaussian Bandpass Receive Filter

The above discussions assume that an ideal matched filter is used prior to the phase and amplitude detectors. We now consider the use of a practical narrowband IF Gaussian bandpass filter in place of a matched filter. Due to limited bandwidth, intersymbol interference (ISI) is introduced. Our aim is to find out what IF receive filter bandwidth should be chosen in order that the system performance can be optimized in terms of minimal BER. In this paper, we will consider a Gaussian bandpass filter whose low-pass equivalent transfer function is [9]

$$H(f) = \exp\left(-\pi f^2/2B^2\right) \quad (18)$$

where B is the IF equivalent noise bandwidth. This is a fairly common model for filters used in data transmission since its bell-shaped frequency response is typical of the form encountered in practice and it yields smooth transitions between the signaling levels. Since the speed of fading process is slow compared to the symbol rate $1/T$ so that it remains relatively constant over a few symbol durations, the effect of IF filtering may then be analyzed in a quasi-static manner leading to the following low-pass equivalent output:

$$\begin{aligned} Z_l(t) &= \sqrt{2P_s}R(t)\exp\left(j\phi(t)\right) + \sqrt{P_d}a_s(t) \\ &\quad \cdot \exp\left(j2\pi f_d t\right)R(t)\exp\left(j\phi(t)\right) + W(t) \end{aligned} \quad (19)$$

where $R(t)$ and $\phi(t)$ are given by

$$R(t)\exp\left(j\phi(t)\right) = s(t) * h(t) \quad (20)$$

in which $h(t)$ is the impulse response of the Gaussian filter defined in (18) and $s(t)$ is the transmitted signal defined in (1). The fading process is represented by $a_s(t)$, the complex Gaussian random process with zero mean and unit power, $\frac{1}{2}\langle|a_s(t)|^2\rangle = 1$. The parameter f_d is the Doppler shift of the specular component as defined in Section III. The Gaussian noise $W(t)$ has the power of $\frac{1}{2}\langle|W(t)|^2\rangle = N_0 B$.

As noted in [8], for $BT \geq 1.0$, $h(t)$ has significant values for a duration of no greater than $2T$ s. To simplify the analysis, we assume that BT (the product of IF filter bandwidth B and the symbol duration T) is sufficiently large so that the ISI effects on any symbol are due solely to the symbol

$$P_{e,\text{amp}} = 0.25 * \begin{pmatrix} 2 + P(D(\Delta r_H) < 0, |r_H, r_H) - P(D(\Delta r_L) < 0, |r_H, r_H) \\ +P(D(\Delta r_H) < 0, |r_L, r_L) - P(D(\Delta r_L) < 0, |r_L, r_L) \\ +P(D(\Delta r_L) < 0, |r_L, r_H) - P(D(\Delta r_H) < 0, |r_L, r_H) \\ +P(D(\Delta r_L) < 0, |r_H, r_L) - P(D(\Delta r_H) < 0, |r_H, r_L) \end{pmatrix}. \quad (16)$$

preceding it and the symbol immediately following it [9]. Since every decision in the differential system uses two adjacent symbols, sequences of four symbols must be considered in the analysis. Each symbol can take on any one of the 16 possible signal constellation points, therefore, the ISI analysis has to take account of 16^4 different kinds of four-symbol patterns. Following the approach in [8], this heavy computational load can be significantly lessened by 70% by exploiting certain error probability invariant properties of the pattern set to the bandlimitation process. More details about this invariant properties are given in the Appendix, which shows that the BER of 16 STAR-QAM can be obtained by averaging over a reduced set Π containing 2160 distinct patterns. For each pattern $\{A_0e^{j\theta_0},\ A_1e^{j\theta_1},\ A_2e^{j\theta_2},\ \text{and} A_3e^{j\theta_3}\}$ in the set Π, the periodic repetition of this four-symbol sequence is used as the message signal to simplify ISI analysis via Fourier series expansion. This signal pattern is shown in Fig. 3 and is written as

$$s(t)=\sum_{n=-\infty}^{+\infty}\sum_{m=0}^{3}A_me^{j\theta_m}p(t-mT+4nT). \tag{21}$$

We apply the Fourier series expansion method as in [8] to (20) over the interval $[0,4T]$ to get

$$R(t)\exp(j\phi(t))=\sum_k\{\Omega_k\exp(j2k\pi t/4T)H(k/4T)\} \tag{22}$$

where

$$\begin{aligned}\Omega_k&=\frac{1}{4T}\int_0^{4T}s(t)\exp(-j(2k\pi t/4T))\,dt\\&=\frac{1}{4}\left[\frac{\sin(k\pi/4)}{k\pi/4}\right]\sum_{m=0}^{3}A_me^{j(\theta_m-(2m+1)k\pi/4)}.\end{aligned} \tag{23}$$

In employing the four-symbol pattern technique described above, there is one issue that needs to be addressed. The evaluation of (22) requires all harmonics of $R(t)\exp(j\phi(t))$ to be summed. In practice, the summation can be closely approximated by summing over only a finite number of terms due to the low-pass nature of $h(t)$ and $s(t)$. The sum in (22) may be computed with sufficient accuracy by the approximation [8]

$$R(t)\exp(j\phi(t))\cong\sum_{k=-K}^{K}\{\Omega_k\exp(j2k\pi t/4T)H(k/4T)\} \tag{24}$$

where $6BT\le k\ (\text{integer})<6BT+1$.

In the phase detection for each four-symbol pattern, the correct decision region now is

$$\Delta\theta-\pi/8<\Delta\varphi<\Delta\theta+\pi/8$$

where

$$\Delta\theta=\theta_2-\theta_1=\{m\pi/4,m=0-7\}.$$

Therefore, two error half planes consist of distinct regions in Fig. 2 according to the variation of in different patterns. The rotation angle χ of the two half planes is $3\pi/8-\Delta\theta$ and $-3\pi/8-\Delta\theta$, respectively.

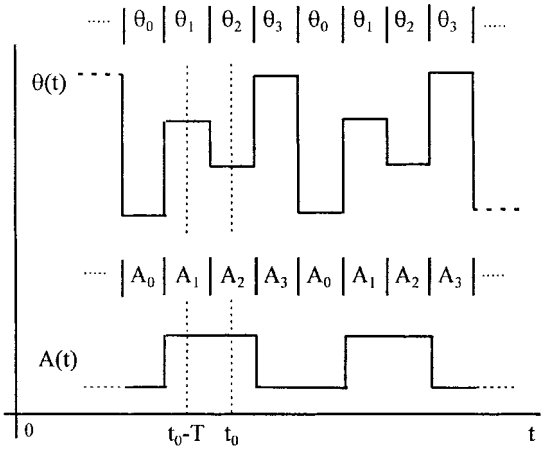

Fig. 3. Waveforms of a typical four-symbol sequence.

The SNR is defined as

$$\frac{E_b}{N_0}=\frac{(P_s+P_d)BT}{4P_n}=\text{SNR}\cdot\frac{BT}{4}.$$

It is to be noted that $\xi_n(T)$ is not zero for the Gaussian IF filter case. But for the range of $BT\ge 1$, $\xi_n(T)\cong 0$, and we are assuming $\xi_n(T)$ to be zero in our computation. Therefore, given $BT,\ E_b/N_0,\ f_dT,\ f_DT$, and K (Rician fading factor) and setting the sampling time to $t_0=2.5T$, the steps involved in calculating P_b are shown below.

1) Generate the ISI sequence $\{A_0e^{j\theta_0},\ A_1e^{j\theta_1},\ A_2e^{j\theta_2},$ and $A_3e^{j\theta_3}\}$.
2) Compute the values of $R(t_0),\ R(t_0-T)$, and $\Delta\phi=\phi(t_0)-\phi(t_0-T)$ using (23) and (24).
3) Compute the $P_{e,\text{phase}},\ P_{e,\text{amp}}$, and P_b using the method described in Sections III-A–C with the following substitutions of (9):

$$\begin{aligned}R(t_0)&\to A_n\\R(t_0-T)&\to A_{n-1}\\\Delta\phi&\to\Delta\theta_n\\\phi(t_0)&\to\theta_n\\\phi(t_0-T)&\to\theta_{n-1}.\end{aligned}$$

4) Repeat Steps 1)–3) for all four-symbol patterns in the set Π. The overall average BER is the average of P_b of all sequences.

V. Bit-Error Rate Results with Matched Filter Receiver

The bit-error probability of 16 STAR-QAM formulated by (17) is evaluated for different values of $L,\ K,\ f_dT$, and f_DT. In the computation, the Marcum Q function was computed using the recursive formula of McGee [6].

The optimum ring ratio for differential detection for Rayleigh fading, that is $K=0$, has been found to be approximately two [5], and using this optimized ring ratio, the thresholds Δr_L and Δr_H have been evaluated to be

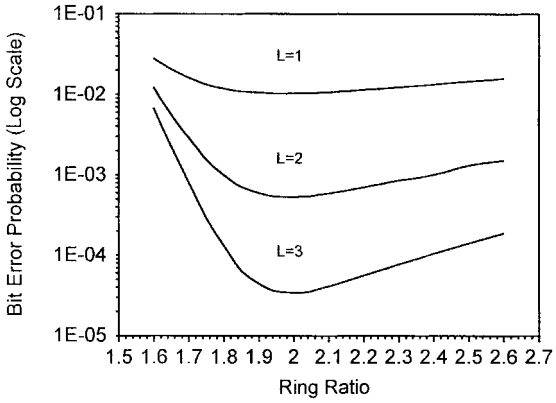

Fig. 4. Bit-error rate versus ring ratio for various values of L with $f_DT = 0$, $f_dT = 0$, $E_b/N_0 = 15$ dB, and $K = 5$ dB.

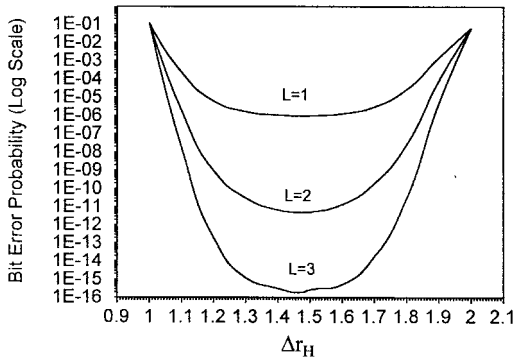

Fig. 5. Bit-error rate versus Δr_H for various values of L with $f_DT = 0$, $f_dT = 0$, $E_b/N_0 = 30$ dB, and $K = 10$ dB.

equal to 0.68 and 1.47, respectively [5]. For Rician fading, the optimum set of ring ratio and thresholds for different values of L, K, and f_DT have not been found previously and is searched in the present work. First, the Δr_H value is fixed to be equal to 1.47, which is the optimum value in the Rayleigh fading channel. Then, the optimum value of the ring ratio is searched. A ring ratio of approximately two is needed for optimum performance, as shown in Fig. 4. Using this optimum ring ratio of two, the optimum values of Δr_L and Δr_H in Rician fading channel are searched. The optimum value of Δr_H is evaluated to be equal to 1.47. This is clearly illustrated in Fig. 5. Δr_L is set to be $1/\Delta r_H = 0.68$. The authors noticed that the optimum ring ratio and Δr_H changes slightly with large variations of the K Rician factor and SNR. For most cases, the combination of (2.0, 1.47) gives the best BER performance.

The computed BER's for 16 STAR-QAM in Rician fading as a function of L, K, and f_DT are plotted in Figs. 6 and 7. The BER curves for the case of Rayleigh fading $(K = 0)$ are also shown in Fig. 6 for comparison. As expected, the BER at first drops off with increasing E_b/N_0, in conformity with the usual behavior of BER in an AWGN channel. As E_b/N_0 becomes very large, the BER levels off to constant floor values indicating the influence of random FM noise. It is also noted that reception diversity lowers the error floors significantly.

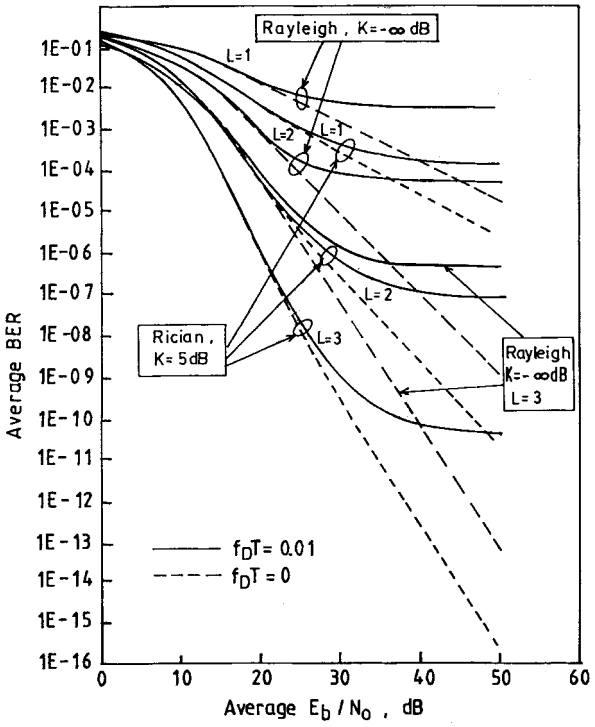

Fig. 6. Bit-error rate of 16 STAR-QAM in Rician fading for various values of L with $f_DT = 0$ and 0.01 and $f_dT = 0$.

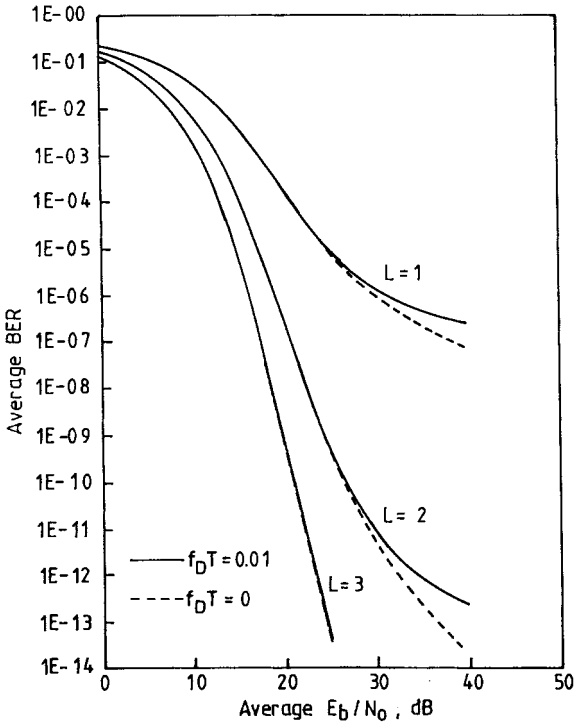

Fig. 7. Bit-error rate of 16 STAR-QAM in Rician fading for various values of L with $f_DT = 0$ and 0.01 and $K = 10$ dB and $f_dT = 0$.

Recently, Chow *et al.* [11] presented an error-bound analysis for M-ary differential phase-shift keying (MDPSK) in fading channels with diversity reception. For MDPSK, naturally, due to the fact that all the signal points are on one ring, no amplitude detection is necessary. In this paper, we have

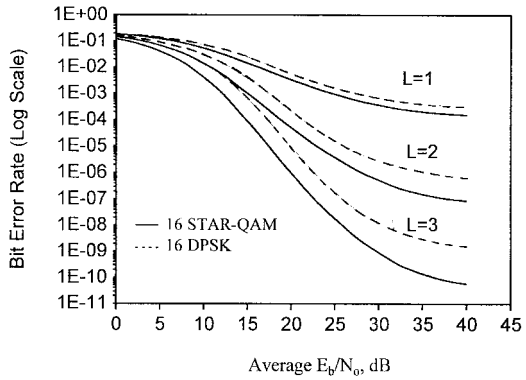

Fig. 8. Bit-error rate of 16 STAR-QAM and 16 DPSK in Rician fading for various values of L with $f_DT = 0.01$, $f_dT = 0$, and $K = 5$ dB.

computed the BER for 16 DPSK with the method described in Section III-A. The results are compared with those for the 16 STAR-QAM in Fig. 8 for $f_DT = 0.001$, $K = 5$ dB, and for various values of L. It is interesting to note that 16 STAR-QAM outperforms 16 DPSK quite significantly for the same power-limited condition. For example, for $E_b/N_0 = 40$ dB, $L = 2$, the BER for 16 DPSK is 6.7×10^{-7}. At these parameter values, the BER for 16 STAR-QAM is 8.8×10^{-8}. This improvement is to be expected because the range for a correct phase decision in the case of 16 STAR-QAM is larger than that for 16 DPSK. From the results obtained, it seems that the additional amplitude detection required for the 16 STAR-QAM does not lead to a severe performance degradation than if the additional bit were encoded in the additional degree of phase modulation as in the case of 16 DPSK. Nevertheless, one must bear in mind that the detector and decoder circuitry for 16 STAR-QAM is much more complex than that for the 16 DPSK. Finally, 16 STAR-QAM requires a linear power amplifier, whereas 16 DPSK does not.

When Doppler shift is present $(f_dT \neq 0)$, the BER performance becomes worse as shown in Fig. 9. The difference of the BER with and without Doppler shift is more pronounced in the case of a higher order diversity.

VI. Bit-Error Rate Results with Narrowband Gaussian IF Filter

In the presence of ISI, error rates for various values of BT have been calculated with different L, K, and f_DT by using the procedure described in Section IV. These are shown in Figs. 10–13. The optimum ring ratio was searched to be 2.0, and Δr_H was searched to be 1.47 as was for the case of a matched filter receiver. There will be less ISI when BT is large, while more Gaussian noise is added to the signal because of the wider filter bandwidth. Therefore, an optimum BT can be found to give an optimal BER performance.

As observed in Figs. 10–13, an optimum BT is found to be around 1.2 depending on the values of L and K (less sensitive to variations in K) in the range of SNR, where AWGN has a large influence, that is, in the region of SNR before the appearance of error-rate floors.

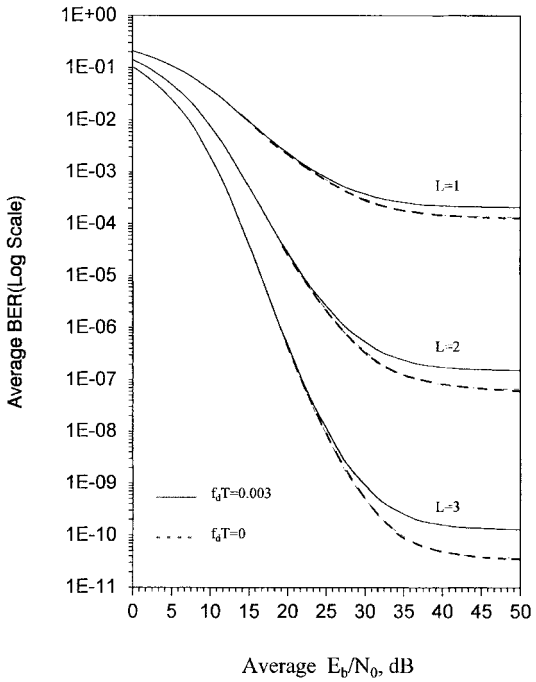

Fig. 9. Bit-error rate of 16 STAR-QAM in Rician fading for various values of L with $f_DT = 0.01$ and $K = 5$ dB.

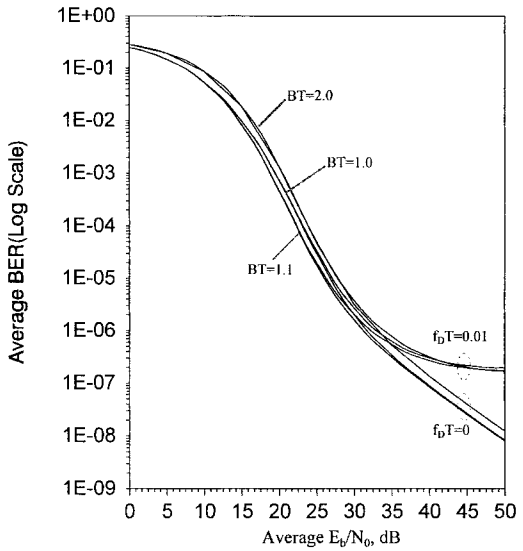

Fig. 10. Bit-error rate of 16 STAR-QAM with ISI effect, $f_dT = 0$, $K = 10$ dB, and $L = 1$.

In the range of large SNR, where error floor appears, the effect of AWGN can be neglected. As can be seen in Fig. 12, since a larger BT leads to less ISI, a better performance of large BT's will be observed as the average E_b/N_0 becomes large. This behavior of BER as a function of BT has also been discussed in [10]. As shown in Fig. 10, f_DT determines the irreducible BER value. The larger the f_DT value, the more severe is the effect of random phase noise. In summary, higher BER floor values are obtained for smaller BT values and larger f_DT values. However, the BER floor value is less sensitive to variations in BT as compared to the variations in f_DT.

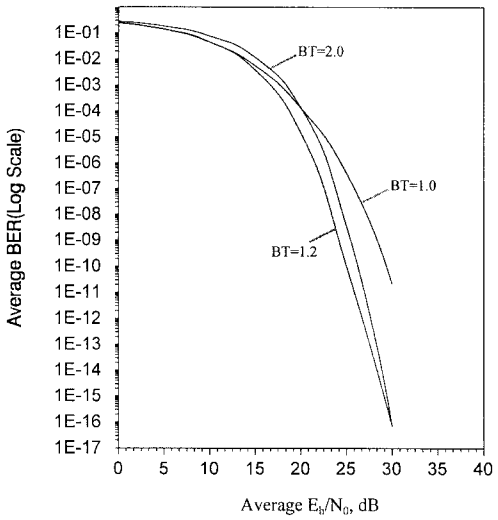

Fig. 11. Bit-error rate of 16 STAR-QAM with ISI effect, $K = 20$ dB, $L = 1$, $f_dT = 0$, and $f_DT = 0.01$.

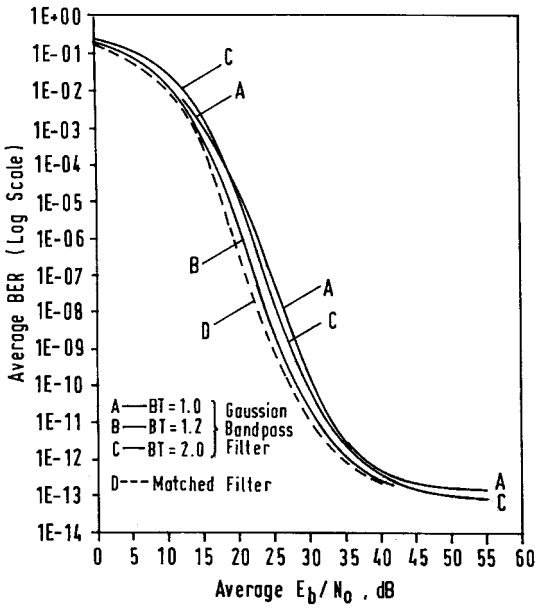

Fig. 12. Bit-error rate of 16 STAR-QAM in Rician fading with ISI effect, $K = 10$ dB, $L = 2$, $f_dT = 0$, and $f_DT = 0.01$.

Comparing Fig. 10 with Fig. 11 and Fig. 12 with Fig. 13, as K increases, the effect of the value of BT is more prominent. This is because the channel is more similar to an AWGN channel when K is large. That is, the fading contributes a smaller diffused component in the received signal. Consequently, a more noticeable BER difference with respect to various BT can be seen in the figures, as expected of the influence of an AWGN.

Finally, for comparison, we have also plotted in Fig. 12 the BER curve for the matched filter case (curve D). As expected, the matched filter provides the lowest BER, but it is interesting to note that when the Gaussian filter bandwidth is judiciously chosen, say $BT = 1.2$, the BER performance of the Gaussian IF filter case is not much different from that of the matched filter receiver.

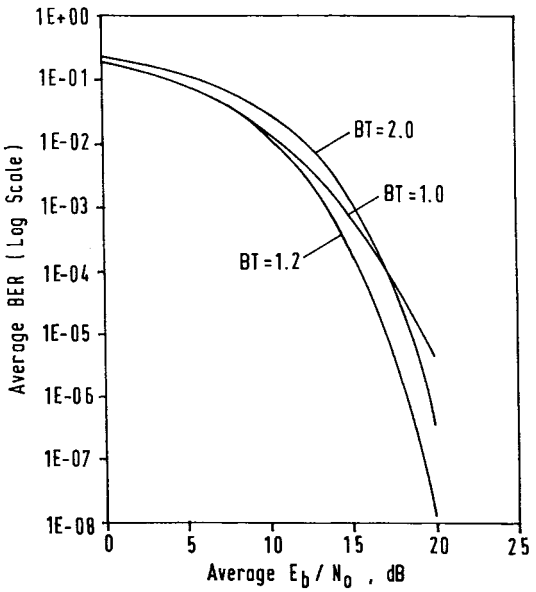

Fig. 13. Bit-error rate of 16 STAR-QAM in Rician fading with ISI effect, $K = 20$ dB, $L = 2$, $f_dT = 0$, and $f_DT = 0.01$.

VII. Conclusions

In this paper, we have derived the expression for the bit-error probability for the 16 STAR-QAM systems in a Rician fading channel in the presence of ISI with diversity reception and presented the BER performance curves for various values of K, Doppler spreading frequencies, IF filter bandwidths, and the orders of the diversity reception. We have also compared its performance with that of the 16 DPSK. The 16 STAR-QAM system can be used optimally in a digital mobile cellular system if BT is set to be around 1.2.

Appendix
P_b Invariant Four-Symbol Patterns

In this Appendix, we will illustrate the error probability invariant properties of certain four-symbol patterns. As stated in Section IV, to take into account the effect of ISI introduced through $R(t)$ and $\phi(t)$, the average bit-error probability P_b is computed using bit-error probabilities from a reduced set Π of 2160 four-symbol patterns instead of from the initial set of 16^4 patterns. This is due to the fact that some patterns in the original set have the same bit-error probabilities and can therefore be combined into a group and represented by one pattern in this group. P_b invariant properties describe what kinds of patterns produce the same BER and hence belong to the same group.

Applying the substitutions given in Section IV to (7)–(9), it can be seen that $P(D<0, |R(t_0), R(t_0-T))$ depends only on parameters of a, b, v_1, and ν_2, while a and b are determined by ν_1, ν_2, α_1, and α_2. Thus, the error probability depends solely on ν_1, ν_2, α_1, and α_2. A close examination of (8) and (9) shows that interchanging $R(t_0)$ and $R(t_0-T)$ does not affect the value of ν_1, ν_2, α_1, and α_2. Besides, it can also be observed that ν_1, ν_2, α_1, and α_2 depend on the phase difference $|\Delta\theta - \Delta\phi|$ (note $\chi = \pm 3\pi/8 - \Delta\theta$). Consequently,

the effect of ISI on average error probability P_b is reflected in the pair $(R(t_0), R(t_0 - T))$ and $|\Delta\theta - \Delta\phi|$.

Given

$$\vartheta = \{A_0 e^{j\theta_0}, A_1 e^{j\theta_1}, A_2 e^{j\theta_2}, A_3 e^{j\theta_3}\} \in \Pi$$

the waveform of this four-symbol pattern is shown in Fig. 3 and has the expression of (21). With $H(f)$ being an even function of f and the error probability having the above mentioned characteristic, it can be shown by using (23) and (24) that the following four transformations of ϑ have the same error probability.

A. Conjugate Four-Symbol Pattern

$$\begin{aligned}
\vartheta_1 &= \{A_0 e^{-j\theta_0}, A_1 e^{-j\theta_1}, A_2 e^{-j\theta_2}, A_3 e^{-j\theta_3}\} \\
s_1(t) &= \overline{s(t)} \\
R_1(t) e^{j\phi_1(t)} &= s_1(t) * h(t) \\
R_1(t_0) &= R(t_0) \quad R_1(t_0 - T) = R(t_0 - T) \\
\phi_1(t_0) &= -\phi(t_0) \quad \phi_1(t_0 - T) = -\phi(t_0 - T) \\
|\Delta\theta_1 - \Delta\phi_1| &= |\Delta\theta - \Delta\phi|.
\end{aligned}$$

B. Time-Reversed Four-Symbol Pattern

$$\begin{aligned}
\vartheta_2 &= \{A_3 e^{j\theta_3}, A_2 e^{j\theta_2}, A_1 e^{j\theta_1}, A_0 e^{j\theta_0}\} \\
s_2(t) &= s(2t_0 - T - t) \\
R_2(t) e^{j\phi_2(t)} &= s_2(t) * h(t) \\
R_2(t_0) &= R(t_0 - T) \quad R_2(t_0 - T) = R(t_0) \\
\phi_2(t_0) &= \phi(t_0 - T) \quad \phi_2(t_0 - T) = \phi(t_0) \\
|\Delta\theta_2 - \Delta\phi_2| &= |\Delta\theta - \Delta\phi|.
\end{aligned}$$

C. Phase-Reversed Four-Symbol Pattern

$$\begin{aligned}
\vartheta_3 &= \{A_0 e^{j(\pi/4 - \theta_0)}, A_1 e^{j(\pi/4 - \theta_1)}, A_2 e^{j(\pi/4 - \theta_2)} \\
&\qquad A_3 e^{j(\pi/4 - \theta_3)}\} \\
s_3(t) &= e^{j2G} \overline{s(t)} \quad G = \pi/8 \\
R_3(t) e^{j\phi_3(t)} &= s_3(t) * h(t) \\
R_3(t_0) &= R(t_0) \quad R_3(t_0 - T) = R(t_0 - T) \\
\phi_3(t_0) &= 2G - \phi(t_0) \quad \phi_3(t_0 - T) = 2G - \phi(t_0 - T) \\
|\Delta\theta_3 - \Delta\phi_3| &= |\Delta\theta - \Delta\phi|.
\end{aligned}$$

D. Phase Offset Four-Symbol Pattern

$$\begin{aligned}
\vartheta_4 &= \{A_0 e^{j(P + \theta_0)}, A_1 e^{j(P + \theta_1)}, A_2 e^{j(P + \theta_2)} \\
&\qquad A_3 e^{j(P + \theta_3)}\} \\
s_4(t) &= e^{jP} s(t) \\
R_4(t) e^{j\phi_4(t)} &= s_4(t) * h(t) \\
R_4(t_0) &= R(t_0) \quad R_4(t_0 - T) = R(t_0 - T) \\
\phi_4(t_0) &= P + \phi(t_0) \quad \phi_4(t_0 - T) = P + \phi(t_0 - T) \\
|\Delta\theta_4 - \Delta\phi_4| &= |\Delta\theta - \Delta\phi|.
\end{aligned}$$

The pattern set can now be combined in a manner such that any member within a group can be transformed into another member within the same group through a combination of the conjugate, time-reversing, phase-reversing, and phase-offsetting operations described above. Members of set Π are searched through a computer program from the original 16^4 patterns.

REFERENCES

[1] P. J. Lee, "Computation of the bit error rate of coherent M-ary PSK with gray code bit mapping," *IEEE Trans. Commun.*, vol. COM-34, pp. 488–491, May 1986.

[2] J. G. Proakis, " On the probability of error for multichannel reception of binary signals," *IEEE Trans. Commun. Technol.*, vol. COM-16, pp. 68–71, Feb. 1968.

[3] F. Adachi and M. Sawahashi, "Performance analysis of various 16 level modulation schemes under Rayleigh fading," *Electron. Lett.*, vol. 28, pp. 1579–1581, Aug. 1992.

[4] Y. C. Chow, A. R. Nix, and J. P. McGeehan, "Analysis of 16-APSK modulation in AWGN and Rayleigh fading channel," *Electron. Lett.*, vol. 28, pp. 1608–1610, Aug. 1992.

[5] ——, "Diversity improvement for 16-DAPSK in Rayleigh fading channel," *Electron. Lett.*, vol. 29, pp. 387–389, Feb. 1993.

[6] W. F. McGee, "Another recursive method of computing the Q-function," *IEEE Trans. Inform. Theory*, vol. 17, pp. 500–501, July 1970.

[7] P. B. Kennington, R. J. Wilkinson, and J. D. Marvill, "A multi-carrier amplifier for future mobile communications systems," in *IEE 6th Int. Conf. Mobile Radio and Personal Communications*, Dec. 9–11, 1991, Univ. Warwick, U.K., pp. 151–156.

[8] C. S. Ng, P. S. Chin, T. T. Tjhung, and K. M. Lye, "Closed-form error probability formula for narrowband DQPSK in slow Rayleigh fading and Gaussian noise," *IEICE Trans. Commun.*, vol. E75-B, no. 5, pp. 401–412, 1992.

[9] R. F. Pawula, "On the theory of error rates for narrow-band digital FM," *IEEE Trans. Commun.*, vol. COM-29, pp. 1634–1643, Nov. 1981.

[10] C. S. Ng, T. T. Tjhung, F. Adachi, and P. S. Chin, "Closed-form error probability formula for narrow-band FSK, with limiter-discriminator-integrator detection, in Rayleigh fading," *IEEE Trans. Commun.*, vol. 42, pp. 2795–2802, Oct. 1994.

[11] Y. C. Chow, J. P. McGeehan, and A. R. Nix, "Simplified error bound analysis for M-DPSK in fading channels with diversity reception," *Proc. Inst. Elect. Eng. Commun.*, vol. 141, no. 5, pp. 341–350, 1994.

[12] W. C. Jakes, Jr., *Microwave Mobile Communications*. New York: Wiley, 1974, p. 21.

Tjeng Thiang Tjhung (SM'84) received the B.Eng. and M.Eng. degrees in electrical engineering from Carleton University, Ottawa, Ont., Canada, in 1963 and 1965, respectively, and the Ph.D. degree from Queen's University, Kingston, Ont., in 1969.

From 1963 to 1968, he worked with Acres-InterTel. Ltd., Ottawa, as a Consultant, where his work was concerned with FSK systems for secure radio communication. In 1969, he joined the Department of Electrical Engineering, National University of Singapore, Singapore, where he is currently a Professor. His present research interests are in bandwidth-efficient digital modulation techniques for mobile radio and in coherent optical fiber communication systems. From 1977 to 1983, he was a Consultant to Singapore Telecom on the planning and implementation of their optical fiber wideband network.

Dr. Tjhung is a Member of the IEICE Japan and a Fellow of IES Singapore. He is also a Member of the Association of Professional Engineers of Singapore.

Xiaodai Dong received the B.Eng. degree in information and control engineering from Xi'an Jiaotong University, P.R.C., in 1992 and the M.Eng. degree in electrical engineering from National University of Singapore, Singapore, in 1995. She is currently pursuing the Ph.D. degree at the Department of Electrical and Computer Engineering, Queen's University, Kingston, Canada.

Her research interests are digital mobile communication and coding.

Fumiyuki Adachi (M'79–SM'90) received the Dr.Eng. degree from Tohoku University, Japan, in 1984.

In 1973, he joined Nippon Telegraph & Telephone Corporation (NTT) Laboratories, Yokosuka-shi, Kanagawa-ken, Japan, and in 1992 he transferred to NTT Mobile Communications Networks, Inc. At NTT, he worked for the development of a TDMA digital cellular base-station transceiver. Presently, he is a Senior Executive Research Engineer at NTT Mobile Communications Networks, Inc. and has been leading a research group for wideband DS-CDMA cellular radio. During the academic year of 1984/85, he was a United Kingdom SERC Visiting Research Fellow in the Department of Electrical and Electronics Engineering, Liverpool University, Liverpool, U.K. He has written chapters of three books: *Fundamentals of Mobile Communications* (Japan: IEICE, 1986), *Mobile Communications* (Japan: Maruzen, 1989), and *Digital Mobile Communications* (Japan: Kagaku Shinbun-sha, 1992). His present research interests also include bandwidth-efficient digital modulation/demodulation, diversity reception, and channel coding.

Dr. Adachi was a Secretary of the IEEE Vehicular Technology Society Tokyo Chapter from 1991 to 1994 and was a Corecipient of the IEEE Vehicular Technology Society Paper of the Year Award in 1980 and 1990.

Kang Hai Tan was born in Malaysia on June 18, 1969. He received the B.Eng. (Honors) degree in electrical engineering from the National University of Singapore, Singapore, in 1994.

He is now with Lucent Technologies Singapore as a Senior Cellular Engineer. His primary function is in designing and optimizing new AMPS and CDMA cellular telephone systems.